Stabilization of the epitaxial rhombohedral ferroelectric phase in ZrO_2 by surface energy

Ali El Boutaybi,* Thomas Maroutian, Ludovic Largeau, Sylvia Matzen, and Philippe Lecoeur
Centre de Nanosciences et de Nanotechnologies, Universite Paris-Saclay, CNRS, 91120 Palaiseau, France

(Received 10 November 2021; revised 21 February 2022; accepted 28 June 2022; published 25 July 2022)

Doped HfO_2 and HfO_2-ZrO_2 compounds are gaining significant interest thanks to their ferroelectric properties in ultrathin films. Here, we show that ZrO_2 could be a playground for doping and strain engineering to increase the thickness in epitaxial thin films. Based on surface-energy considerations supported by *ab initio* calculations, we find that pure ZrO_2 exhibits a ferroelectric rhombohedral phase (r phase, with $R3m$ space group) more stable than for the HZO and pure HfO_2 cases. In particular, for a thickness up to 37 nm we experimentally evidence a single (111)-oriented r phase in ZrO_2 films deposited on $La_{2/3}Sr_{1/3}MnO_3$-buffered $DyScO_3$(110) substrate. The formation of this r phase is discussed and compared between HfO_2, ZrO_2 and HZO, highlighting the role of surface energy.

DOI: 10.1103/PhysRevMaterials.6.074406

I. INTRODUCTION

Since the discovery of ferroelectricity in Si-doped hafnia in 2011 [1], hafnia-based thin films have been widely studied to stabilize the ferroelectric phase, and many polar phases have been suggested or experimentally proved. In polycrystalline thin films, the orthorhombic phase $Pbc2_1$ is usually reported [1,2]. Theoretically, two other polar phases were found for HfO_2, an orthorhombic $Pnm2_1$ [3,4] and a rhombohedral $R3$ [5]. The main problem observed in polar orthorhombic is the necessity of a high number of applied electric-field cycles (the so-called wake-up effect) to reach the ferroelectric state [6–8]. Moreover, two other issues that are often encountered in these polycrystalline films are the degradation of the ferroelectricity with the increase of film thickness, with a vanishing polarization above a thickness of about 20 nm [1,9,10], and the coexistence of nonpolar phases such as monoclinic and tetragonal phases with the polar one [11,12]. Indeed, HfO_2 as well as ZrO_2 are well known for their structural and chemical similarity [13], and both of them can adopt a wide variety of crystal phases. In bulk form and at room temperature, the stable phase is monoclinic (m phase, $P2_1/c$). At high temperature, tetragonal phase (t phase, $P42/nmc$) and cubic phase (c phase, $Fm3m$) are observed for ZrO_2 and HfO_2 [14,15]. The noncentrosymmetric, ferroelectric orthorhombic $Pbc2_1$ phase (o phase) can be obtained via transformation of the t phase under stress [16–18], or under tensile strain [19]. On the other hand, in 2018, Wei *et al.* [20] demonstrated the rhombohedral symmetry with $R3m$ space group (r phase) for the first time in epitaxial $Hf_{0.5}Zr_{0.5}O_2$ (HZO) thin films under compressive strain on a $La_{2/3}Sr_{1/3}MnO_3$ (LSMO)-buffered $SrTiO_3$(001) substrate (STO), and no wake-up effect was observed. Strain engineering is thus investigated to stabilize this r phase on different substrates, such as recently demonstrated by Zheng *et al.* for HZO epitaxial films on ZnO [21].

The influence of surface energy on phase stability has been discussed in polycrystalline films through studies on grain size. It was shown that optimizing the latter could stabilize the orthorhombic $Pbc2_1$ ferroelectric phase in pure HfO_2 [22] and ZrO_2 [23], and that inserting different interlayers allowed the ferroelectricity to be maintained above 40-nm thickness in HZO [24,25]. Concerning bulk ceramics and polycrystalline films, it is known that for a grain diameter less than 30 nm, the ZrO_2 adopts the t phase [26,27], whereas the HfO_2 has a similar size effect at around 5 nm [11,28]. From this perspective, ZrO_2-based epitaxial thin films are promising to increase both film thickness and grain size, which are usually critical for energy storage [29] and optical applications [30–32]. Mastering the surface-energy balance during growth is thus identified as a critical issue to control the ferroelectric phases of hafnia and zirconia compounds [33,34]. However, very few data are available regarding actual surface energies of the polar and nonpolar phases [35], and as far as we know no data concerning surface energy were reported for the rhombohedral polar phase.

The rhombohedral phase in ZrO_2 or partially stabilized zirconia (PSZ) has been known for more than two decades. Hasegawa [36] reported a rhombohedral phase in the abraded surfaces of PSZ and fully stabilized zirconia powders; this phase was only observed in the surface layer under some stress, which can be introduced by polishing and grinding. It was therefore postulated that the rhombohedral phase could only exist in the presence of stress. Also, this rhombohedral phase has been reported as an intermediate phase during cubic and tetragonal-monoclinic transformation [37–39]. Nevertheless, in all these earlier studies, no electric properties were reported. $R3m$ and $R3$ rhombohedral phases were evidenced in HZO epitaxial thin films [20,21,40], and recently, Silva *et al.* [41] reported the same r phase in an 8-nm-thick ZrO_2 thin film deposited on Nb-STO(111). While this polar r phase is promising for numerous applications based on ultrathin films [42–45], the issue of its poor thickness-dependent stability is still present when increasing the thickness above 10 nm.

*ali.el-boutaybi@c2n.upsaclay.fr

 ©2022 American Physical Society

In this picture, we will show that rhombohedral ZrO_2 films are more stable at high thickness than HfO_2 and HZO ones, and thus that ZrO_2-rich compounds provide a playground for strain engineering and doping schemes towards outstanding ferroelectric properties.

In this work, we first compare with the support of *ab initio* calculations the stability of the (111)-oriented rhombohedral *R*3*m* phase between pure ZrO_2, HZO, and pure HfO_2. We then study epitaxial ZrO_2, HZO, and HfO_2 thin films grown by pulsed laser deposition (PLD) on both (110)-oriented $DyScO_3$ (DSO) and (001)-oriented STO substrates, with LSMO buffer. Using x-ray diffraction (XRD), we evidence the presence of the *r* phase in ZrO_2 thin films, up to about 40-nm thickness, with a clear ferroelectric behavior without wake-up effect.

II. RESULTS AND DISCUSSION

We performed density-functional theory (DFT) calculations to investigate the (111)-oriented rhombohedral stability by employing the QUANTUM ESPRESSO package [46] with Perdew-Burke-Ernzerhof [47] generalized gradient approximation (see Supplemental Material (SM) for more details [48]). First, we ran our calculations for *m*-, *t*-, *o*-, and *r* phases of ZrO_2, HZO, and HfO_2. The energies of these phases are summarized in Table S1 with a comparison to literature data. Our results agree with previous calculations using different approaches and with the experimental results. For *r*-ZrO_2, we obtained an energy of 140 meV/f.u. with respect to the monoclinic energy, which is less than the 154 meV/f.u. found for *r*-HfO_2, in good agreement with Ref. [20]. In a second step, the calculations for different surface orientations were performed by constructing four-layer-thick slabs separated by 15 Å of vacuum (more details in SM. [48]). We note that no bottom electrode was included in these calculations. It is known that the surfaces on each side of a slab may interact through long-range strain fields induced by ionic relaxations [49]. This effect depends somewhat on surface orientation and on the material; for metals, for example, the interlayer relaxations typically fall below the experimental threshold after three to four layers [50]. Orlando *et al.* [51] showed the same average value in the case of *t*-ZrO_2. Thus, slabs of four layers were used for surface-energy calculations (Fig. S2) with a $5 \times 5 \times 1$ *k*-point sampling in the surface Brillouin zone [52], and an energy cutoff of 60 Ry.

The surface energy in joule per square meter is given in Table S2 and Fig. 1 for (111)-oriented *m*- and *r* phases at different ratios of ZrO_2 in $Hf_{1-x}Zr_xO_2$ composition. The $r-(111)$ showed the lowest surface energy compared to all other calculated surfaces of HfO_2, ZrO_2, and HZO. This is in agreement with the fact that the (111) atomic planes of the *r* phase appear more flat and dense than, e.g., the (-111) *m*-phase ones (Fig. S2). As indicated in Fig. 1, (-111) *m* phase increases in energy with increasing ZrO_2 content, while the *r*-(111) surface energy decreases. This, in turn, increases the energy gap between the *m*-(-111) and *r*-(111) surfaces, with this gap achieving its maximum in pure ZrO_2. Note that the surface energy of *m*-(111) was also calculated and it showed a value higher but close to that of *m*-(-111), in line with previous calculations reported in Ref. [49].

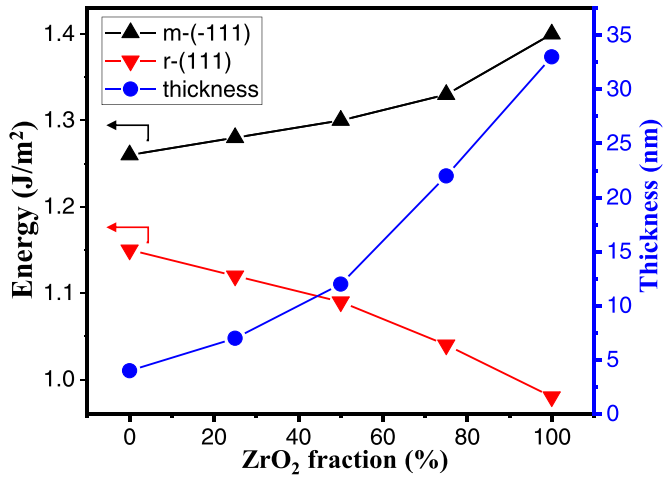

FIG. 1. Surface energy of *m*- and *r* phase of $Hf_{1-x}Zr_xO_2$ ($x = 0$, 0.25, 0.50, 0.75, and 1) shown in black and red, respectively. The thickness up to which Gibbs energy of the *R*3*m* phase is lower than the one of the m phase is shown in blue.

In the literature, the role of the surface energy was not systematically explored in HfO_2-ZrO_2 epitaxial thin films, especially regarding the stabilization of the rhombohedral phase. In order to assess the relative stability of the *m*- and *r* phases, taking into account the computed surface energies, we use a simple thermodynamic argument based on the Gibbs free energy [33], that was successfully applied to explain the stability of the orthorhombic polar phase in atomic layer deposited thin films [11,33]. Figure 1 shows (in blue) the thickness up to which the Gibbs free energy of the *r* phase is lower than the one of the *m* phase as a function of ZrO_2 content in $Hf_{1-x}Zr_xO_2$. This estimated maximum thickness for the *r* phase was calculated with an in-plane compressive strain of 1%, which is close to the estimated strain from our experimental results as shown below. The stability window of *r*-ZrO_2 is up to a thickness of 33 nm, while it is less than 4 nm in pure HfO_2. For HZO, the rhombohedral phase is stable up to a thickness of about 12 nm, in good agreement with previous results that reported a 10-nm maximum thickness in epitaxial HZO thin films [20]. The (111)-oriented HfO_2 *R*3*m* phase was discussed elsewhere [53] and found to be stable at a very low thickness (two layers) compared to the (111)-orthorhombic and (111)-monoclinic. Thus, from our calculations, pure ZrO_2 epitaxial thin films are expected to be the most stable regarding the (111)-oriented *R*3*m* phase. This makes ZrO_2-based thin films very promising to stabilize the rhombohedral polar phase at significantly higher thickness than reported for HZO.

In order to test our findings experimentally, ZrO_2, HfO_2, and $Hf_{0.5}Zr_{0.5}O_2$ films were grown by PLD on LSMO-buffered DSO and STO substrates. The ferroelectric nature of ZrO_2 and HZO was characterized through Positive Up Negative Down measurements on capacitor devices with Pt top and LSMO bottom electrodes on DSO substrate (more details are given in SM. [48]). In 14-nm-thick films, remanent polarizations (2Pr) of 40 and 41.5 $\mu C/cm^2$ were measured for HZO and ZrO_2, respectively (Fig. S4). These results are comparable to the previously reported values in epitaxial HZO

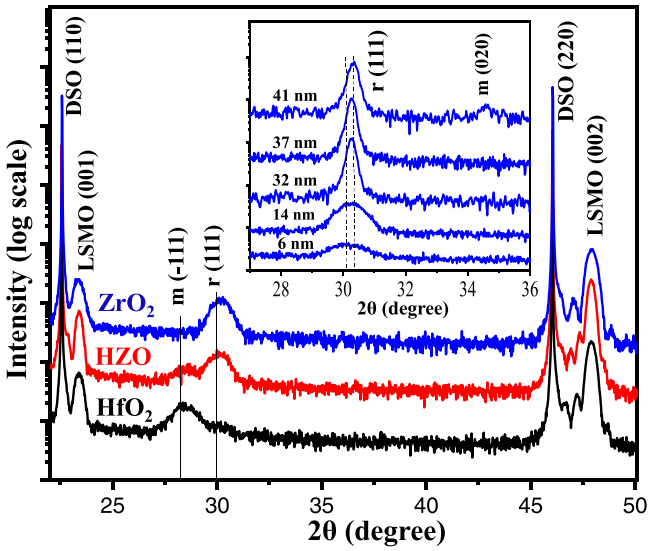

FIG. 2. Out-of-plane XRD θ–2θ scans of HZO, HfO_2, and ZrO_2 films on LSMO-buffered 110-oriented DSO with thicknesses of 14 nm. Inset figure shows θ–2θ of ZrO_2 at different thicknesses, and dashed lines show the 2θ shift of the (111)-ZrO_2 diffraction peak.

with the same range of thickness [20,54,55]. At 37-nm thickness, a 2Pr of 22 $\mu C/cm^2$ is measured for pure ZrO_2 [Fig. S4(c)], hinting at a persistent ferroelectricity.

Structural analyses were performed by XRD with Panalytical X'pert Pro diffractometer for out-of-plane θ–2θ scans (Fig. 2) and Rigaku SmartLab diffractometer equipped with a rotating anode for in-plane measurements and pole figure (Fig. 3). Figure 2 gives θ–2θ patterns of HZO, HfO_2, and ZrO_2 films at a thickness of 14 nm. The highest peaks correspond to the (110)-oriented orthorhombic DSO substrate. At the right and close to the substrate peaks are the LSMO peaks corresponding to (001) pseudocubic orientation. The thickness of LSMO is about 25 nm, measured by x-ray reflectivity. For 2θ between 30.09 °–30.27 °, is found the (111) peak of the HfO_2, HZO, and ZrO_2 films. Note that the diffracted peak around 30 ° is referred to the (111) orthorhombic $Pbc2_1$ in polycrystalline thin films [1], and even in some epitaxial thin films [54]. In the case of polycrystalline films this peak is usually found at a slightly higher 2θ value (around 30.5 °) compared to epitaxial thin films [10]. Here, the (111) diffracted peak will be ascribed to the rhombohedral phase, as demonstrated below through complementary XRD analyses. In the case of pure HfO_2, a peak at 2θ around 28.3° is observed

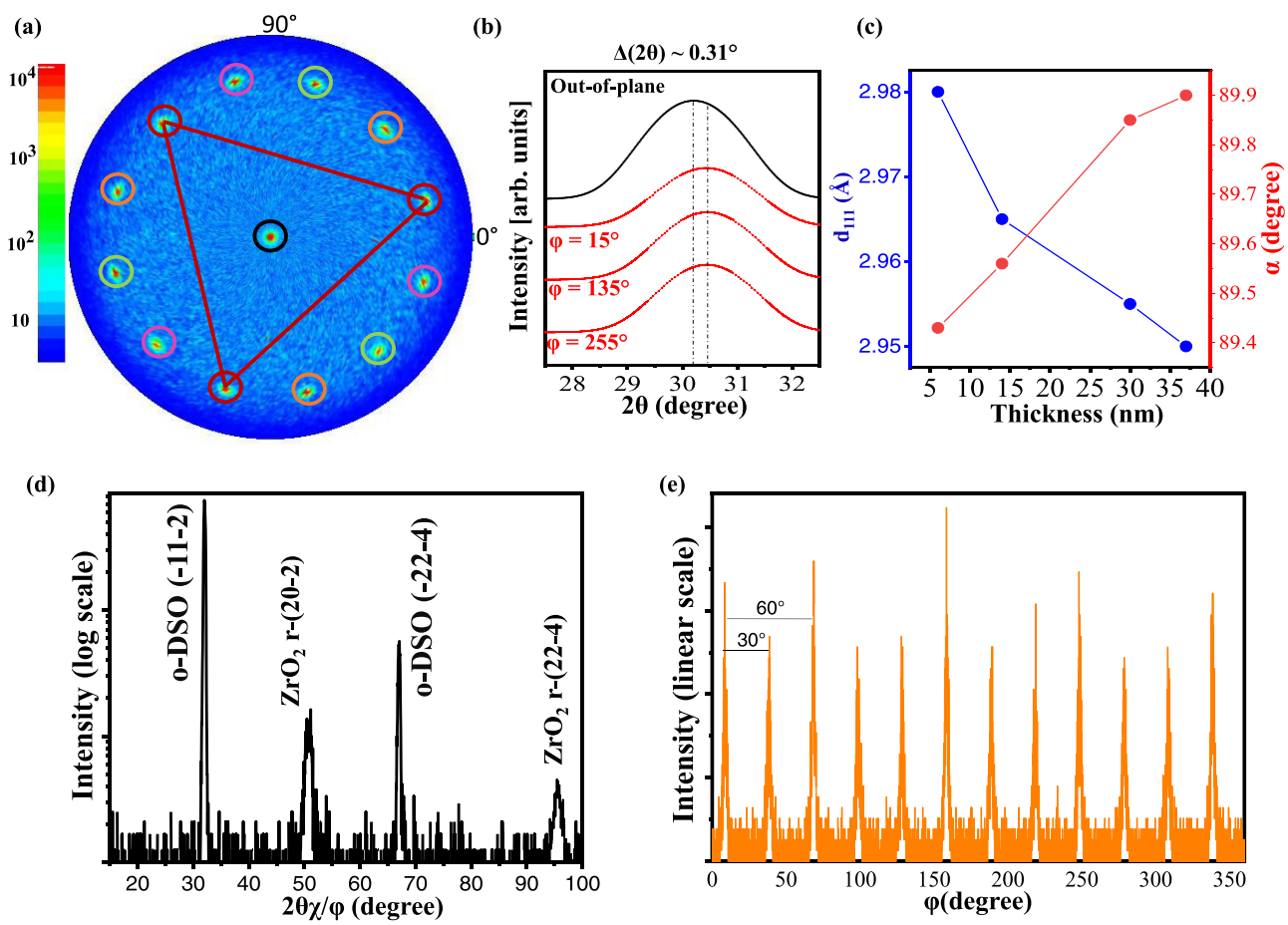

FIG. 3. (a) Pole figure around the (111) peak at $2\theta = 30.19°$ of a 14-nm-thick ZrO_2 film. The radial angle χ varies between 0 ° and 90 °; the azimuthal angle φ is in the 0 °–360 ° range. (b) θ–2θ scans of one r variant (red circles in pole figure) revealing a $\Delta(2\theta)$ shift of 0.31 ° between diffraction peaks corresponding to out-of-plane and 71 °-inclined {111} planes. (c) Out-of-plane d_{111} and rhombohedral angle α at various thicknesses. (d) In-plane $2\theta\chi/\varphi$ scan along $(-11-2)$ DSO in-plane azimuthal direction. (e) In-plane φ scan around $2\theta\chi = 50.54°$.

with higher intensity than r-(111); this peak corresponds to (-111) m phase [56]. This m-(-111) peak decreases in intensity in HZO film and disappears in pure ZrO_2 film. The inset of Fig. 2 shows the XRD data of pure ZrO_2 films at different thicknesses. The r phase in the film appears compressively strained, as the (111) peak is shifted towards smaller angles for the thinner films, indicating that the out-of-plane parameter is expanded compared to the relaxed one at 41 nm. From this thickness-dependent shift, a compressive strain of around 1% was extracted [48]. Additionally, a diffraction peak at 34.6° attributed to the m-(020) plane is observed in the 41-nm-thick ZrO_2 film [56], while no monoclinic phase is observed for thicknesses up to 37 nm. Noteworthy, an increase in compressive strain higher than 1% could increase the thickness of the pure r-ZrO_2 film much higher than 37 nm.

In line with our theoretical considerations, both our experimental composition and thickness series confirm that a polar (111)-oriented phase remains stable at high thickness upon increasing the ZrO_2 content in HfO_2-ZrO_2 compounds, allowing to reach a thickness close to 40 nm in pure ZrO_2 on DSO substrate. We now present the additional XRD measurements that unambiguously identify the rhombohedral phase in our ZrO_2 thin films, as previously reported for HZO films [20]. Note that due to the very low intensity of the r-phase related peak in our pure HfO_2 films (Fig. 2, black), we could not perform a similar analysis for them.

Figure 3(a) shows a pole figure for a 14-nm-thick ZrO_2 film on DSO substrate measured at $2\theta = 30.19°$; 12 radial peaks were found, corresponding to four variants of ZrO_2. For one r-ZrO_2 variant, only three peaks are expected at a radial angle $\chi = 71°$ [48]. The three inclined planes diffract at a different angle than the (111) plane (surface plane of the thin film), which gives a multiplicity of 3:1, that is a feature of rhombohedral symmetry. Figure 3(b) shows θ–2θ scans for {-111} planes family of one rhombohedral variant (selected in red in pole figure) inclined relatively to the sample surface: A clear shift between these peaks collected at $\chi \sim 71°$ and the one corresponding to the (111) plane parallel to the surface is observed, confirming the rhombohedral symmetry [20]. The shift between the central peak and the inclined ones is around $\Delta(2\theta) = 0.31°$, and the same shift was observed for the other variants (Fig. S5). Importantly, with d_{hkl} the interplanar spacing of (hkl) planes, the d_{111}–d_{11-1} difference depends on the α angle of the rhombohedral phase. An angle $\alpha = 89.40°$ was reported in HZO thin film with a thickness of 5.9 nm [40], and $\alpha = 89.5°$ in ZrO_2-3% Y_2O_3 powder [38], which gives a $\Delta(2\theta)$ between the r-(111) and r-{-111} planes of about 0.42° and 0.36°, respectively. According to the shift observed in Fig. 3(b), the estimated angle for 14-nm-thick pure ZrO_2 r phase is $\alpha = 89.56°$ with lattice parameters $a = b = c \approx 5.089$ Å. The values of α and of the corresponding out-of-plane d_{111} at different thicknesses of ZrO_2 films are reported in Fig. 3(c). They exhibit a clear dependence on thickness, characteristic of the relaxation of an in-plane compressively strained r phase: The angle α increases toward 90° and d_{111} decreases as the film thickness increases. This relaxation is consistent with the decrease of polarization measured in ZrO_2 films between 14- and 37-nm thickness (Fig. S4). Indeed, compressive strain was shown to have a strong impact on the ferroelectric properties of the r phase [20,40,53].

In order to get further insights into the epitaxial relationships of ZrO_2 films on LSMO-buffered DSO and STO, and to be more sensitive to the eventual presence of minority phases, we performed a series of in-plane XRD measurements. These in-plane measurements were done only for HZO (SM [48]) and pure ZrO_2 films; as in pure HfO_2, the dominant phase is monoclinic. First, we searched the (-11-2) plane of orthorhombic DSO (o-DSO) substrate that diffracts at around $2\theta = 32.09°$ (called $2\theta\chi$ in in-plane geometry) by rotating the sample in plane along the φ angle [57]. That allows to fix the offset between $2\theta\chi$ and φ. Then, in-plane $2\theta\chi/\varphi$ scans were performed along the azimuthal substrate directions, as given in Fig. 3(d). In addition to the substrate peaks, two other peaks are present at $2\theta\chi = 50.54°$ and $2\theta\chi = 95.57°$, which correspond to the rhombohedral (20-2) and (22-4) planes, respectively. As the (22-4) plane is rotated by 30° relative to the (20-2) plane, in fact, from Fig. 3(d), two rhombohedral variants rotated by 90° against each other are observed [Fig. S7(c)]. In order to determine the in-plane symmetry of the ZrO_2 phase, we performed in-plane φ scans with the detector fixed at $2\theta\chi = 50.54°$. The φ scan is shown in Fig. 3(e), revealing 12 peaks with a separation $\Delta\varphi = 30°$, confirming the sixfold symmetry (hexagonal notation) of ZrO_2 thin film. The φ scan for $2\theta\chi = 95.57°$ and the substrate are given in SM (Fig. S6), also indicating a sixfold symmetry of the peak around 95.57°. Similar results were obtained for HZO thin film (Fig. S7 in SM. [48]). Finally, we note that no LSMO peak was detected in the in-plane scans, neither on DSO nor on STO substrate, in agreement with a fully strained LSMO buffer layer [58].

Furthermore, growth of ZrO_2 and HZO films on STO substrate was also tested and the same structural analyses as discussed for DSO substrate were performed. Interestingly, a tetragonal phase has been detected along the r phase by in-plane measurements (Figs. S9 and S10). The in-plane lattice parameters calculated from XRD for this phase are $a = b \approx 5.088$ Å, close to the value reported for the relaxed t-ZrO_2 [59,60]. This t phase was not observed on DSO substrate neither in out-of-plane nor in in-plane XRD scans, even at the highest studied thicknesses of ZrO_2 thin films (Fig. 2), hinting at an effect of the different strain caused by DSO compared to STO substrate on t-phase stability.

III. CONCLUSION

In conclusion, the rhombohedral phase in HfO_2-ZrO_2 compounds was systematically studied using first-principles calculations and experiments. We evidenced the increasing stability of (111)-oriented r phase with ZrO_2 content from surface-energy considerations, and demonstrated experimentally the stabilization of this pure rhombohedral phase in a 37-nm-thick ZrO_2 thin film deposited on LSMO-buffered DSO (110) substrate, with a remanent polarization $2P_r$ of about 22 $\mu C/cm^2$. On STO (001) substrate, a relaxed tetragonal phase was found to coexist with rhombohedral phase in HZO and pure ZrO_2 films. We believe that ZrO_2-rich epitaxial thin films open routes in terms of strain engineering and doping for optimized ferroelectric properties and thicknesses higher than the ones reported in this work.

ACKNOWLEDGMENTS

This work has received support from the Agence nationale de la recherche (ANR) under project FOIST (Grant No. ANR-18-CE24-0030), and from the French national network RENATECH for nanofabrication. The authors thank Michel Rerat (IPREM-Pau University, France) for helpful discussions on our *ab initio* calculations.

[1] T. S. Böscke, J. Müller, D. Bräuhaus, U. Schröder, and U. Böttger, Ferroelectricity in hafnium oxide thin films, Appl. Phys. Lett. **99**, 102903 (2011).

[2] S. J. Kim, J. Mohan, S. R. Summerfelt, and J. Kim, Ferroelectric $Hf_{0.5}Zr_{0.5}O_2$ thin films: A review of recent advances, JOM **71**, 246 (2019).

[3] T. D. Huan, V. Sharma, G. A. Rossetti, and R. Ramprasad, Pathways towards ferroelectricity in hafnia, Phys. Rev. B **90**, 064111 (2014).

[4] Y. Qi, S. Singh, C. Lau, F.-T. Huang, X. Xu, F. J. Walker, C. H. Ahn, S.-W. Cheong, and K. M. Rabe, Stabilization of Competing Ferroelectric Phases of HfO_2 under Epitaxial Strain, Phys. Rev. Lett. **125**, 257603 (2020).

[5] S. V. Barabash, Prediction of new metastable HfO_2 phases: Toward understanding ferro- and antiferroelectric films, J. Comput. Electron. **16**, 1227 (2017).

[6] F. P. G. Fengler, M. Hoffmann, S. Slesazeck, T. Mikolajick, and U. Schroeder, On the relationship between field cycling and imprint in ferroelectric $Hf_{0.5}Zr_{0.5}O_2$, J. Appl. Phys. **123**, 204101 (2018).

[7] M. Pešić, F. P. G. Fengler, L. Larcher, A. Padovani, T. Schenk, E. D. Grimley, X. Sang, J. M. LeBeau, S. Slesazeck, U. Schroeder, and T. Mikolajick, Physical mechanisms behind the field-cycling behavior of HfO_2-based ferroelectric capacitors, Adv. Funct. Mater. **26**, 4601 (2016).

[8] M. Lederer, R. Olivo, D. Lehninger, S. Abdulazhanov, T. Kämpfe, S. Kirbach, C. Mart, K. Seidel, and L. M. Eng, On the origin of wake-up and antiferroelectric-like behavior in ferroelectric hafnium oxide, Phys. Status Solidi RRL **15**, 2100086 (2021).

[9] M. H. Park, H. J. Kim, Y. J. Kim, W. Lee, T. Moon, K. D. Kim, and C. S. Hwang, Study on the degradation mechanism of the ferroelectric properties of thin $Hf_{0.5}Zr_{0.5}O_2$ films on TiN and Ir electrodes, Appl. Phys. Lett. **105**, 072902 (2014).

[10] M. Hyuk Park, H. Joon Kim, Y. Jin Kim, W. Lee, T. Moon, and C. Seong Hwang, Evolution of phases and ferroelectric properties of thin $Hf_{0.5}Zr_{0.5}O_2$ films according to the thickness and annealing temperature, Appl. Phys. Lett. **102**, 242905 (2013).

[11] M. H. Park, Y. H. Lee, H. J. Kim, T. Schenk, W. Lee, K. D. Kim, F. P. G. Fengler, T. Mikolajick, U. Schroeder, and C. S. Hwang, Surface and grain boundary energy as the key enabler of ferroelectricity in nanoscale hafnia-zirconia: A comparison of model and experiment, Nanoscale **9**, 9973 (2017).

[12] J. Müller, U. Schröder, T. S. Böscke, I. Müller, U. Böttger, L. Wilde, J. Sundqvist, M. Lemberger, P. Kücher, T. Mikolajick, and L. Frey, Ferroelectricity in yttrium-doped hafnium oxide, J. Appl. Phys. **110**, 114113 (2011).

[13] R. Ruh and P. W. R. Corfield, Crystal structure of monoclinic hafnia and comparison with monoclinic zirconia, J. Am. Ceram. Soc. **53**, 126 (1970).

[14] J. Wang, H. P. Li, and R. Stevens, Hafnia and hafnia-toughened ceramics, J. Mater. Sci. **27**, 5397 (1992).

[15] X. Luo, W. Zhou, S. V. Ushakov, A. Navrotsky, and A. A. Demkov, Monoclinic to tetragonal transformations in hafnia and zirconia: A combined calorimetric and density functional study, Phys. Rev. B **80**, 134119 (2009).

[16] E. H. Kisi, Influence of hydrostatic pressure on the t → o transformation in Mg-PSZ studied by in situ neutron diffraction, J. Am. Ceram. Soc. **81**, 741 (1998).

[17] A. H. Heuer, V. Lanteri, S. C. Farmer, R. Chaim, R. R. Lee, B. W. Kibbel, and R. M. Dickerson, On the orthorhombic phase in ZrO_2-based alloys, J. Mater. Sci. **24**, 124 (1989).

[18] P. Fan, Y. K. Zhang, Q. Yang, J. Jiang, L. M. Jiang, M. Liao, and Y. C. Zhou, Origin of the intrinsic ferroelectricity of HfO_2 from ab initio molecular dynamics, J. Phys. Chem. C **123**, 21743 (2019).

[19] S. J. Lee, M. J. Kim, T. Y. Lee, T. I. Lee, J. H. Bong, S. W. Shin, S. H. Kim, W. S. Hwang, and B. J. Cho, Effect of ZrO_2 interfacial layer on forming ferroelectric $Hf_xZr_yO_z$ on Si substrate, AIP Adv. **9**, 125020 (2019).

[20] Y. Wei, P. Nukala, M. Salverda, S. Matzen, H. J. Zhao, J. Momand, A. S. Everhardt, G. Agnus, G. R. Blake, P. Lecoeur, B. J. Kooi, J. Íñiguez, B. Dkhil, and B. Noheda, A rhombohedral ferroelectric phase in epitaxially strained $Hf_{0.5}Zr_{0.5}O_2$ thin films, Nat. Mater. **17**, 1095 (2018).

[21] M. Zheng, Z. Yin, Y. Cheng, X. Zhang, J. Wu, and J. Qi, Stabilization of thick, rhombohedral $Hf_{0.5}Zr_{0.5}O_2$ epilayer on c-plane ZnO, Appl. Phys. Lett. **119**, 172904 (2021).

[22] K. D. Kim, M. H. Park, H. J. Kim, Y. J. Kim, T. Moon, Y. H. Lee, S. D. Hyun, T. Gwona, and C. S. Hwang, Ferroelectricity in undoped-HfO_2 thin films induced by deposition temperature control during atomic layer deposition, J. Mater. Chem. C **4**, 6864 (2016).

[23] S. Starschich, T. Schenk, U. Schroeder, and U. Boettger, Ferroelectric and piezoelectric properties of $Hf_{1-x}Zr_xO_2$ and pure ZrO_2 films, Appl. Phys. Lett. **110**, 182905 (2017).

[24] S. Riedel, P. Polakowski, and J. Müller, A thermally robust and thickness independent ferroelectric phase in laminated hafnium zirconium oxide, AIP Adv. **6**, 095123 (2016).

[25] H. J. Kim, M. H. Park, Y. J. Kim, Y. H. Lee, W. Jeon, T. Gwon, T. Moon, K. D. Kim, and C. S. Hwang, Grain size engineering for ferroelectric $Hf_{0.5}Zr_{0.5}O_2$ films by an insertion of Al_2O_3 interlayer, Appl. Phys. Lett. **105**, 192903 (2014).

[26] R. C. Garvie, The occurrence of metastable tetragonal zirconia as a crystallite size effect, J. Phys. Chem. **69**, 1238 (1965).

[27] M. W. Pitcher, S. V. Ushakov, A. Navrotsky, B. F. Woodfield, G. Li, J. Boerio-Goates, and B. M. Tissue, Energy crossovers in nanocrystalline zirconia, J. Am. Ceram. Soc. **88**, 160 (2005).

[28] M. Shandalov and P. C. McIntyre, Size-dependent polymorphism in HfO_2 nanotubes and nanoscale thin films, J. Appl. Phys. **106**, 084322 (2009).

[29] M. H. Park, H. J. Kim, Y. J. Kim, T. Moon, K. D. Kim, and C. S. Hwang, Thin $Hf_xZr_{1-x}O_2$ films: A new lead-free system for electrostatic supercapacitors with large energy storage density

and robust thermal stability, Adv. Energy Mater. **4**, 1400610 (2014).

[30] D. K. Fork, F. Armani-Leplingard, and J. J. Kingston, Optical losses in ferroelectric oxide thin films: Is there light at the end of the tunnel? MRS Online Proc. Library **361**, 155 (1994).

[31] B. W. Wessels, Ferroelectric oxide epitaxial thin films: Synthesis and non-linear optical properties, J. Cryst. Growth **195**, 706 (1998).

[32] D. Sando, Y. Yang, C. Paillard, B. Dkhil, L. Bellaiche, and V. Nagarajan, Epitaxial ferroelectric oxide thin films for optical applications, Appl. Phys. Rev. **5**, 041108 (2018).

[33] R. Materlik, C. Kunneth, and A. Kersch, The origin of ferroelectricity in $Hf_{1-x}Zr_xO_2$: A computational investigation and a surface energy model, J. Appl. Phys. **117**, 134109 (2015).

[34] T. Mimura, T. Shimizu, and H. Funakubo, Ferroelectricity in $YO_{1.5}$-HfO_2 films around 1 μm in thickness, Appl. Phys. Lett. **115**, 032901 (2019).

[35] R. Batra, H. D. Tran, and R. Ramprasad, Stabilization of metastable phases in hafnia owing to surface energy effects, Appl. Phys. Lett. **108**, 172902 (2016).

[36] H. Hasegawa, Rhombohedral phase produced in abraded surfaces of partially stabilized zirconia (PSZ), J. Mater. Sci. Lett. **2**, 91 (1983).

[37] H. Hasegawa, T. Hioki, and O. Kamigaito, Cubic-to-rhombohedral phase transformation in zirconia by ion implantation, J. Mater. Sci. Lett. **4**, 1092 (1985).

[38] O. N. Grigor'ev, G. S. Krivoshei, N. A. Stel'mashenko, V. I. Trefilov, and A. V. Shevchenko, Phase transformations during mechanical treatment and the properties of surface layers of a zirconium dioxide ceramic, Sov. Powder Metall. Met. Ceram. **30**, 376 (1991).

[39] D. P. Burke and W. M. Rainforth, Intermediate rhombohedral (r-ZrO_2) phase formation at the surface of sintered Y-TZP's, J. Mater. Sci. Lett. **16**, 883 (1997).

[40] L. Bégon-Lours, M. Mulder, P. Nukala, S. de Graaf, Y. A. Birkhölzer, B. Kooi, B. Noheda, G. Koster, and G. Rijnders, Stabilization of phase-pure rhombohedral $HfZrO_4$ in pulsed laser deposited thin films, Phys. Rev. Materials **4**, 043401 (2020).

[41] J. P. B. Silva, R. F. Negrea, M. C. Istrate, S. Dutta, H. Aramberri, J. Íñiguez, F. G. Figueiras, C. Ghica, K. C. Sekhar, and A. L. Kholkin, Wake-up free ferroelectric rhombohedral phase in epitaxially strained ZrO_2 thin films, ACS Appl. Mater. Interfaces **13**, 51383 (2021).

[42] Y. Wei, S. Matzen, T. Maroutian, G. Agnus, M. Salverda, P. Nukala, Q. Chen, J. Ye, P. Lecoeur, and B. Noheda, Magnetic Tunnel Junctions Based on Ferroelectric $Hf_{0.5}Zr_{0.5}O_2$ Tunnel Barriers, Phys. Rev. Applied **12**, 031001 (2019).

[43] Y. Wei, S. Matzen, C. P. Quinteros, T. Maroutian, G. Agnus, P. Lecoeur, and B. Noheda, Magneto-ionic control of spin polarization in multiferroic tunnel junctions, npj Quantum Mater. **4**, 62 (2019).

[44] B. Prasad, V. Thakare, A. Kalitsov, Z. Zhang, B. Terris, and R. Ramesh, Large tunnel electroresistance with ultrathin $Hf_{0.5}Zr_{0.5}O_2$ ferroelectric tunnel barriers, Adv. Electron. Mater. **7**, 2001074 (2021).

[45] J. P. B. Silva, K. C. Sekhar, H. Pan, J. L. MacManus-Driscoll, and M. Pereira, Advances in dielectric thin films for energy storage applications, revealing the promise of group IV binary oxides, ACS Energy Lett. **6**, 2208 (2021).

[46] P. Giannozzi, S. Baroni, N. Bonini, M. Calandra, R. Car, C. Cavazzoni, D. Ceresoli, G. L. Chiarotti, M. Cococcioni, I. Dabo *et al.*, QUANTUM ESPRESSO: A modular and open-source software project for quantum simulations of materials, J. Phys.: Condens. Matter **21**, 395502 (2009).

[47] J. P. Perdew, K. Burke, and M. Ernzerhof, Generalized Gradient Approximation Made Simple, Phys. Rev. Lett. **77**, 3865 (1996).

[48] See Supplemental Material at http://link.aps.org/supplemental/10.1103/PhysRevMaterials.6.074406 for details on *ab initio* calculations, thin film growth, ferroelectric characterizations, and complementary X-ray diffraction data, which includes Refs. [61–76].

[49] A. Christensen and E. A. Carter, First-principles study of the surfaces of zirconia, Phys. Rev. B **58**, 8050 (1998).

[50] T. Ning, Q. Yu, and Y. Ye, Multilayer relaxation at the surface of fcc metals: Cu, Ag, Au, Ni, Pd, Pt, Al, Surf. Sci. **206**, L857 (1988).

[51] R. Orlando, C. Pisani, E. Ruiz, and P. Sautet, *Ab initio* study of the bare and hydrated (001) surface of tetragonal zirconia, Surf. Sci. **275**, 482 (1992).

[52] W. Sun and G. Ceder, Efficient creation and convergence of surface slabs, Surf. Sci. **617**, 53 (2013).

[53] Y. Zhang, Q. Yang, L. Tao, E. Y. Tsymbal, and V. Alexandrov, Effects of Strain and Film Thickness on the Stability of the Rhombohedral Phase of HfO_2, Phys. Rev. Applied **14**, 014068 (2020).

[54] J. Lyu, I. Fina, R. Solanas, J. Fontcuberta, and F. Sánchez, Robust ferroelectricity in epitaxial $Hf_{1/2}Zr_{1/2}O_2$ thin films, Appl. Phys. Lett. **113**, 082902 (2018).

[55] T. Song, H. Tan, N. Dix, R. Moalla, J. Lyu, G. Saint-Girons, R. Bachelet, F. Sánchez, and I. Fina, Stabilization of the ferroelectric phase in epitaxial $Hf_{1-x}Zr_xO_2$ enabling coexistence of ferroelectric and enhanced piezoelectric properties, ACS Appl. Electron. Mater. **3**, 2106 (2021).

[56] A. Gualtieri, P. Norby, J. Hanson, and J. Hriljac, Rietveld refinement using synchrotron X-ray powder diffraction data collected in transmission geometry using an imaging-plate detector: Application to standard m-ZrO_2, J. Appl. Crystallogr. **29**, 707 (1996).

[57] R. P. Liferovich and R. H. Mitchell, A structural study of ternary lanthanide orthoscandate perovskites, J. Solid State Chem. **177**, 2188 (2004).

[58] M. Zahradník, T. Maroutian, M. Zelený, L. Horák, G. Kurij, T. Maleček, L. Beran, Š. Višňovský, G. Agnus, P. Lecoeur, and M. Veis, Electronic structure of $La_{2/3}Sr_{1/3}MnO_3$: Interplay of oxygen octahedra rotations and epitaxial strain, Phys. Rev. B **99**, 195138 (2019).

[59] C. J. Howard, E. H. Kisi, R. B. Roberts, and R. J. Hill, Neutron diffraction studies of phase transformations between tetragonal and orthorhombic zirconia in magnesia-partially-stabilized zirconia, J. Am. Ceram. Soc. **73**, 2828 (1990).

[60] C. J. Howard, R. J. Hill, and B. E. Reichert, Structures of ZrO_2 polymorphs at room temperature by high-resolution neutron powder diffraction, Acta Crystallogr., Sect. B **44**, 116 (1988).

[61] J. E. Jaffe, R. A. Bachorz, and M. Gutowski, Low-temperature polymorphs of ZrO_2 and HfO_2: A density-functional theory study, Phys. Rev. B **72**, 144107 (2005).

[62] I. MacLaren, T. Ras, M. MacKenzie, A. J. Craven, D. W. McComb, and S. De Gendt, Texture, twinning, and metastable

"tetragonal" phase in ultrathin films of HfO_2 on a Si substrate, J. Electrochem. Soc. **156**, G103 (2009).

[63] R. Batra, T. D. Huan, J. L. Jones, G. Rossetti, and R. Ramprasad, Factors favoring ferroelectricity in hafnia: A first-principles computational study, J. Phys. Chem. C **121**, 4139 (2017).

[64] E. H. Kisi and C. J. Howard, Crystal structures of zirconia phases and their inter-relation, Key Eng. Mater. **154**, 1 (1998).

[65] J. E. Lowther, J. K. Dewhurst, J. M. Leger, and J. Haines, Relative stability of ZrO_2 and HfO_2 structural phases, Phys. Rev. B **60**, 14485 (1999).

[66] G. Teufer, The crystal structure of tetragonal ZrO_2, Acta Crystallogr. **15**, 1187 (1962).

[67] J. Müller, T. S. Böscke, U. Schröder, S. Mueller, D. Bräuhaus, U. Böttger, L. Frey, and T. Mikolajick, Ferroelectricity in simple binary ZrO_2 and HfO_2, Nano Lett. **12**, 4318 (2012).

[68] A. V. Radha, O. Bomati-Miguel, S. V. Ushakov, A. Navrotsky, and P. Tartaj, Surface enthalpy, enthalpy of water adsorption, and phase stability in nanocrystalline monoclinic zirconia, J. Am. Ceram. Soc. **92**, 133 (2009).

[69] Z. Zhang, S.-L. Hsu, V. A. Stoica, A. Bhalla-Levine, H. Paik, E. Parsonnet, A. Qualls, J. Wang, L. Xie, M. Kumari, S. Das, Z. Leng, M. McBriarty, R. Proksch, A. Gruverman, D. G. Schlom, L.-Q. Chen, S. Salahuddin, L. W. Martin, and R. Ramesh, Epitaxial ferroelectric $Hf_{0.5}Zr_{0.5}O_2$ with metallic pyrochlore oxide electrodes, Adv. Mater. **33**, 2006089 (2021).

[70] J. Y. Tsao, *Materials Fundamentals of Molecular Beam Epitaxy* (Academic Press, San Diego, 1993).

[71] K. Tapily, J. E. Jakes, D. Gu, H. Baumgart, and A. A. Elmustafa, Nanomechanical study of amorphous and polycrystalline ALD HfO_2 thin films, Int. J. Surf. Sci. Eng. **5**, 193 (2011).

[72] A. Jayaraman, S. Y. Wang, S. K. Sharma, and L. C. Ming, Pressure-induced phase transformations in HfO_2 to 50 GPa studied by Raman spectroscopy, Phys. Rev. B **48**, 9205 (1993).

[73] I. Horcas, R. Fernández, J. M. Gómez-Rodríguez, J. Colchero, J. Gómez-Herrero, and A. M. Baro, WSXM: A software for scanning probe microscopy and a tool for nanotechnology, Rev. Sci. Instrum. **78**, 13705 (2007).

[74] S. Estandía, T. Cao, R. Mishra, I. Fina, F. Sánchez, and J. Gazquez, Insights into the atomic structure of the interface of ferroelectric $Hf_{0.5}Zr_{0.5}O_2$ grown epitaxially on La2/3Sr1/3MnO3, Phys. Rev. Materials **5**, 074410 (2021).

[75] A. Yanase, Y. Segawa, M. Mihara, W. M. Tong, and R. S. Williams, Heteroepitaxial growth of CuCl on MgO(001) substrates, Surf. Sci. **278**, L105 (1992).

[76] M. Grundmann, T. Böntgen, and M. Lorenz, Occurrence of Rotation Domains in Heteroepitaxy, Phys. Rev. Lett. **105**, 146102 (2010).